

3D-Printed Transparent Glass

Du T. Nguyen, Cameron Meyers, Timothy D. Yee, Nikola A. Dudukovic, Joel F. Destino, Cheng Zhu, Eric B. Duoss, Theodore F. Baumann, Tayyab Suratwala, James E. Smay, and Rebecca Dylla-Spears*

Silica inks are developed, which may be 3D printed and thermally processed to produce optically transparent glass structures with sub-millimeter features in forms ranging from scaffolds to monoliths. The inks are composed of silica powder suspended in a liquid and are printed using direct ink writing. The printed structures are then dried and sintered at temperatures well below the silica melting point to form amorphous, solid, transparent glass structures. This technique enables the mold-free formation of transparent glass structures previously inaccessible using conventional glass fabrication processes.

Glass has many appealing properties such as hardness, transparency, thermal resistance, chemical resistance, and chemical tunability. These properties make glass an important material for many chemical, biological, optical, and photonics applications as well as in microfluidic and microelectromechanical systems.^[1–4] As such, there is a drive to achieve features in glass at sub-millimeter length scales or in configurations that are difficult to achieve with conventional glass processing techniques. Additive manufacturing, or 3D printing, has been a transformative technology in many fields, enabling structures with unique properties such as mechanical metamaterials, shape-morphing structures, soft robotics, polymer-derived ceramics, and biomaterial tissue constructs.^[5–10] The ability to 3D print glass structures will enable new functional glass materials that unite the appealing material properties of glasses with tailored, high-resolution architectures.

Several advanced manufacturing methods such as fused deposition, filament feed, binder jetting, and soft replication

molding have been demonstrated for fabricating complex glass structures.^[11–18] However, there are limitations to these methods. In binder jetting, the sintered glasses can be fragile and appear opaque due to incomplete densification. Methods to print glass directly (e.g., fused deposition or filament feed) require high temperatures to melt the silica feedstock, resulting in filaments that are potentially vulnerable to thermal stresses and unable to completely merge into the desired structure, which may limit the printing speed


and resolution of the printed parts. Soft replication molding cannot be used to produce gap-spanning features, and pseudo-3D objects (i.e., stacked assemblies of thin molded sheets) can only be formed by precisely aligning layers that must then be bonded during heat treatment. None of these methods have been shown to produce glasses that are simultaneously transparent, free form, and 3D with sub-millimeter features.

We have developed a two-part process (forming and sintering) which uses direct ink writing (DIW) for the 3D printing of optically transparent glass structures with sub-millimeter features. DIW is a layer-by-layer assembly technique in which shear-thinning inks are extruded through a nozzle in a programmable pattern, upon which the inks rapidly solidify via gelation, evaporation, or temperature-induced phase change.^[19] DIW has been used in a wide range of applications such as polymeric optical wave guides, complex scaffolds, 3D periodic graphene aerogels, and self-healing materials.^[6,20–24] Our process first relies on DIW printing of colloidal silica suspensions to form silica green bodies (porous, low density structures) of the desired shape. A key feature of this process is the ability to control yield stress and shear thinning to obtain ink properties best suited for specific applications of the printed glass. Second, the printed structures are dried and heated to temperatures below the melting point of silica to sinter the green body into a fully dense, amorphous, transparent solid structure (Figure 1). In contrast to direct 3D printing of molten glass, this two-step approach does not require high temperatures during printing and allows for higher resolution features, due to both the ability to extrude thinner filaments and the shrinkage that occurs during the densification stage.

The critical challenges in formulating a suitable ink for formation of the silica green bodies toward glass structures are: i) the ink must possess the desired rheological behavior for printing and shape retention, and ii) the ink must be able to dry without cracking while still maintaining open porosity that

Dr. D. T. Nguyen, T. D. Yee, Dr. N. A. Dudukovic, Dr. J. F. Destino,
Dr. C. Zhu, Dr. E. B. Duoss, Dr. T. F. Baumann, Dr. T. Suratwala,
Dr. R. Dylla-Spears
Lawrence Livermore National Laboratory
Livermore, CA 94550, USA
E-mail: dyllaspears1@llnl.gov

C. Meyers
Department of Earth Sciences
University of Minnesota
Minneapolis, MN 55455, USA
Prof. J. E. Smay
School of Chemical Engineering
Oklahoma State University
Stillwater, OK 74078, USA

 The ORCID identification number(s) for the author(s) of this article can be found under <http://dx.doi.org/10.1002/adma.201701181>.

DOI: 10.1002/adma.201701181

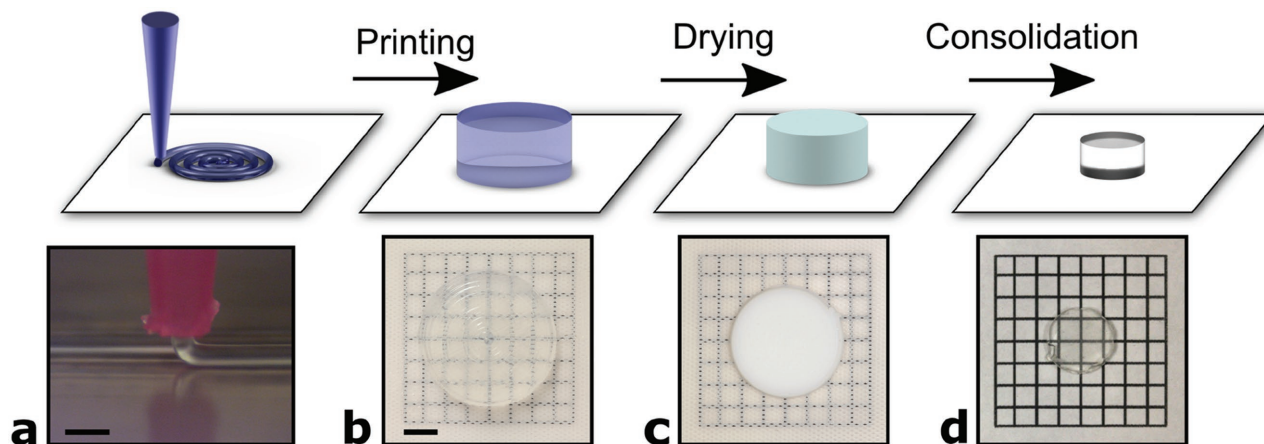


Figure 1. Glass 3D-printing process. a) Silica-filled ink is extruded from a nozzle with the desired resolution (scale bar 500 μm). b) The ink is printed with the desired geometry onto a Teflon mesh to enable the release of the part from the substrate (scale bar 5 mm). c) The printed ink is dried, leaving behind a porous compact of bound silica powder. d) The silica powder is densified at high temperatures to form a transparent, 3D-printed glass part.

allows for complete organic removal and densification. The ink we have developed for the 3D-printing process is a suspension of hydrophilic fumed silica nanoparticles (CAB-O-SIL EH-5) in tetraglyme (tetraethylene glycol dimethyl ether). The fumed silica serves as both the silica source for glass formation as well as the thixotropic agent for the ink. Tetraglyme was chosen for its good dispersion properties for the fumed silica. Additionally, tetraglyme has a high boiling point, enabling the temporal separation of the drying process from the printing operation and allowing for precise control over the drying rate. Hydroxyl-terminated poly(dimethylsiloxane) (PDMS) is added to the ink to help strengthen the network of particles in the

printed form, enhancing crack resistance during the drying of the green bodies.^[25] The silica particle concentration is tuned such that the ink possesses adequate shear-thinning (Figure 2) to be extruded through nozzles with diameters on the order of hundreds of microns as well as a quick viscoelastic recovery upon cessation of flow (Figure S1, Supporting Information). Filaments extruded from inks with higher silica contents retain their extruded shapes well, allowing for the printing of structures with gap-spanning features, such as scaffolds. Filaments extruded from inks with lower silica contents enable the printed filaments to merge and result in monolithic structures without porosity.

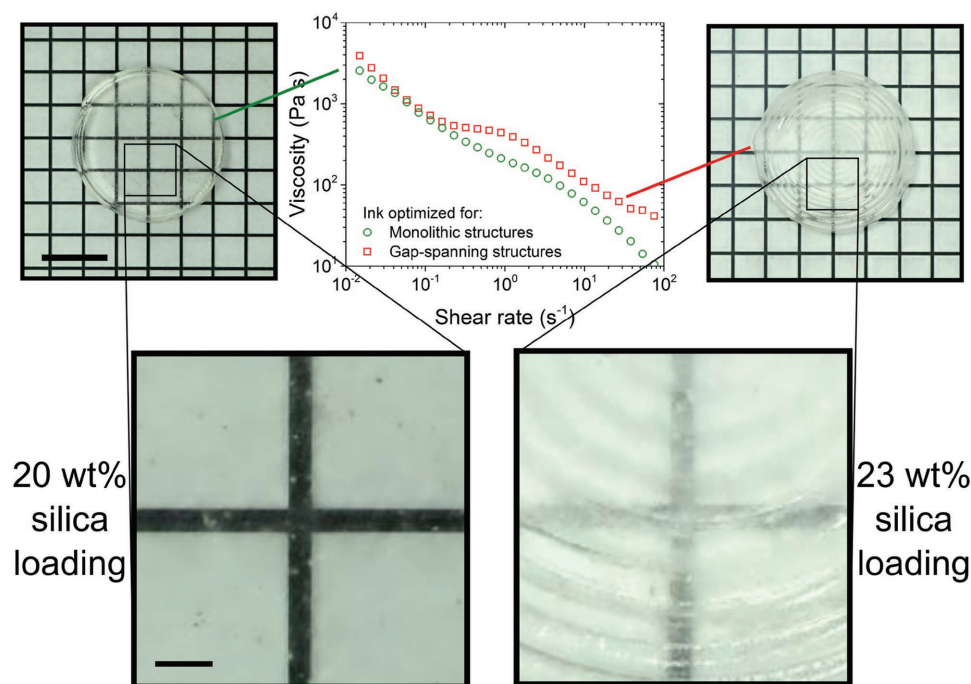


Figure 2. Shear rheology flow curves of silica inks. Increasing the silica content of the ink results in higher viscosity, improved shape retention and enabling of gap-spanning features, but increases print line artifacts in monolithic parts. Scale bar 4 mm (inset 500 μm).

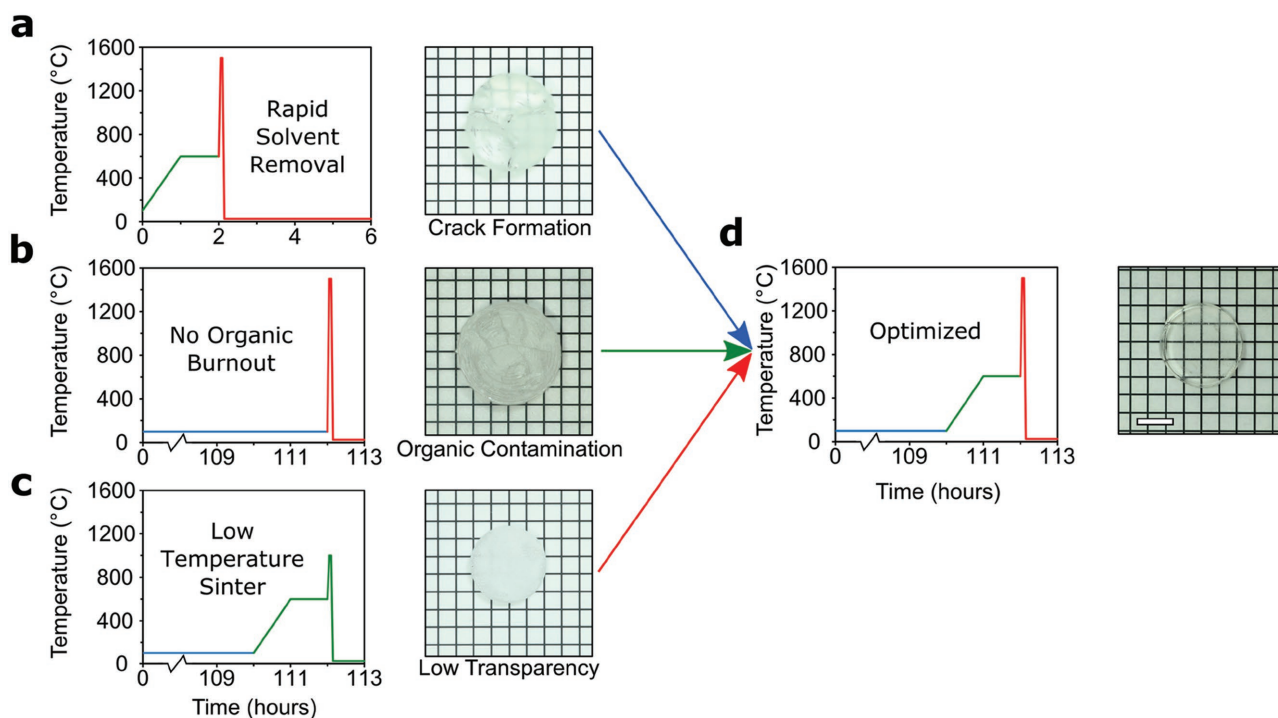


Figure 3. Thermal processing. a) A long drying step at low temperature (100 °C) initially removes the ink solvent. Without the long drying step, crack formation can occur. b) A short step at medium temperature (600 °C) is then used to remove any residual organics. Without the organic burnout, discoloration and crack formation during sintering can occur. c) Last, a rapid step at high sintering temperatures (1500 °C) is used to obtain transparency. Opaque structures result from sintering at lower temperatures. Each step of the densification profile is critical for the formation of crack-free, 3D-printed transparent glass monoliths. 20 wt% silica loading. Scale bar 4 mm.

After printing, the green bodies are subjected to a three-stage heat treatment (**Figure 3**). First, the green bodies must be dried under the proper conditions to remove solvent without degrading the structure. Thermogravimetric analysis of the ink (Figure S2, Supporting Information) indicates that most of the mass loss occurs by 240 °C and is complete by 275 °C, which is the boiling point of tetraglyme. Temperatures ranging from 80–200 °C were explored for drying printed structures; however, temperatures above ≈ 120 °C resulted in crack formation in monoliths. An optimal drying schedule of 100 °C for 110 h was identified for monolithic structures but may be conservative for more open geometries. It is hypothesized that drying at 100 °C makes structures more robust to cracking because the slower rate of mass loss observed below ≈ 110 °C (cf. Figure S2, Supporting Information) allows an increase in green body strength (through network-forming condensation reactions between silica particles) to outpace the rise in capillary pressure due to evaporation.^[26] Further optimization of ink formulation and/or heat treatment could reduce drying times. Following solvent removal, the temperature is raised to 600 °C to complete the second stage of the heat treatment, which involves the burnout of any remaining organics. Without the burnout phase, it is possible for residual organics to become trapped within the glass and result in a poor glass quality upon full densification. During the drying and burnout process, the printed structure shrinks volumetrically by $\approx 43\%$ to form a green body composed solely of chemically bonded silica powder. Third, the green body is densified at 1500 °C in a preheated furnace for

3 min. This results in additional shrinkage as the weakly bound silica structure sinters into a fully dense, transparent glass with a density of 2.2 g cm^{-3} . The total volumetric shrinkage of the print is correlated with the initial volume fraction of silica in the ink, enabling a further reduction in the achievable minimum feature size of the printed parts by this method. For example, the 20 wt% (10 vol%) silica ink results in a final, isotropic, volumetric shrinkage of 90% of the original volume, with consolidated linear feature widths that are $\approx 47\%$ of their printed widths. X-ray diffraction was used to confirm that the process produces amorphous silica glass (Figure S3, Supporting Information). Without careful optimization of the three-staged heat treatment process, the final part can crack, contain entrapped organics, or result in an opaque rather than transparent glass (Figure 3a–c).

We fabricated a variety of structures to demonstrate the versatility of our two-part, 3D-printing and sintering method of glass formation. The most basic structure we fabricated was a solid silica monolith (**Figure 4a**). Extrusion-based 3D-printing processes often lead to visible print line artifacts when fabricating solid structures. Previous work has demonstrated that the rheology of the printing ink can be controlled for either gap spanning or space filling,^[27] which is of importance in creating parts for tailored design. We implemented similar controls to our method to form solid parts without visible print lines, a quality which would be necessary for optical applications. The second structure that we fabricated was a miniaturized glass cup (Figure 4b). In this case, only freestanding cylindrical walls

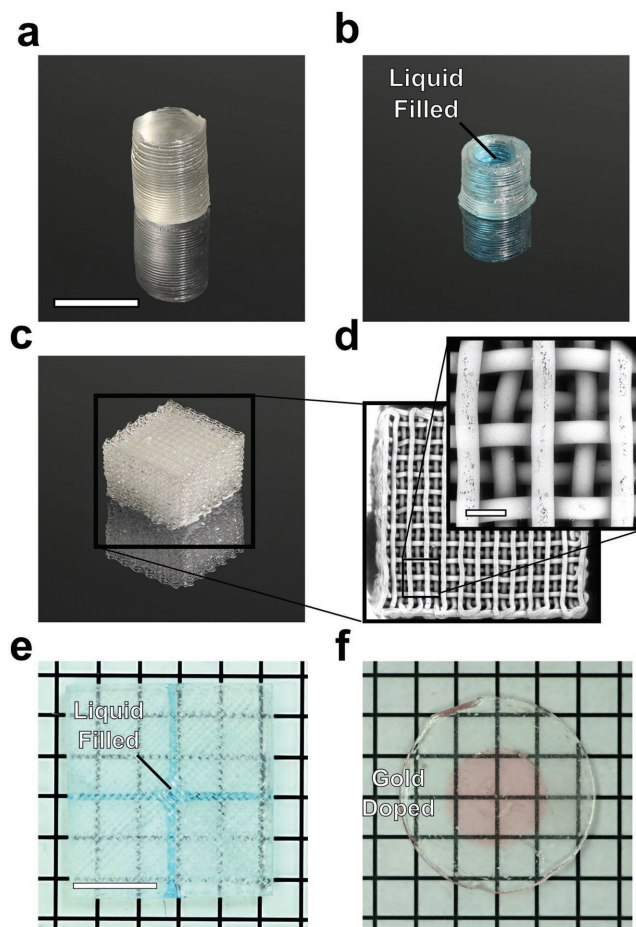


Figure 4. 3D-printed glass structures. a) Solid, monolithic cylinder (20 wt% silica ink). Scale bar 5 mm. b) Cup containing dyed water, highlighting high aspect ratio features (20 wt% silica ink). c) Woodpile scaffold, highlighting gap-spanning features (23 wt% silica ink). d) Scanning electron microscopy of woodpile scaffold. Scale bar 250 μm . e) 3D-printed microfluidic cross junction containing dyed water (23 wt% silica ink). Microfluidic channels are 400 μm wide. Scale bar 4 mm. f) Multicomponent printed glass. Two nozzles containing gold-doped and undoped silica inks are used to print a core-shell structure (20 wt% silica ink). After consolidation into a transparent glass, the gold-doped region retains its red coloration.

were printed, leaving a hollow portion in the center. This structure acted as a rudimentary first step for the printing of glasses for fluidic applications. The cup was filled with liquid without any visible leaking of the liquid, indicating that the merging of individual print lines was suitable for fluidic applications. The walls of the cup demonstrate the ability to print high aspect ratio features using our inks. The third structure we fabricated was a glass face-centered tetragonal scaffold using an ink tuned to have a higher stiffness (23 wt% silica), enabling gap-spanning features (Figure 4c,d). This structure highlights both the small feature size and the spanning elements made possible by our 3D-printing process for glass formation. The initial printed filament diameter was set as 250 μm , and upon consolidation into a transparent glass, the filaments shrank to 140 μm in diameter. Such scaffolds have the potential for use in oil-water separation due to the ability to tune the hydrophilicity

of glass.^[28] Scanning electron microscopy revealed minor surface defects on the structure (Figure 4d); however, the filaments within the bulk of the scaffold were observed to have smooth surfaces. The surface defects are likely due to atmospheric contaminants settling on the green body during the extended drying phase. Another complex geometry that we fabricated was a 3D-printed glass microfluidic cross junction (Figure 4e). Here, the ink was also tuned to have a higher stiffness, enabling the printing of hollow features encased within a bulk shape, in this case a cross-shaped channel. Although print lines were visible, the printed glass microfluidic part was still liquid-tight, demonstrated by flowing dyed water through the microfluidic channels. Further optimization, or the use of two inks (tailored for either gap spanning or space filling) could be used to reduce the visibility of the print lines while still enabling hollow features.

The ability to use DIW for forming glass structures has also opened a route toward printing multi-component glass parts. Our approach provides a facile way of incorporating multiple inks into one structure by adding a second dispensing nozzle to the mechanical stage (Figure 4f). Different variations of the baseline silica ink were used in each nozzle. During the printing of a part, the mechanical stage automatically switches between the two inks, resulting in a multicomponent glass. We demonstrated a two-component glass by combining our silica ink with a gold nanoparticle-doped silica ink. Surface plasmon resonance from the 20 nm gold nanoparticles results in a strong absorption at 528 nm and an apparent red coloration.^[29] The gold nanoparticles and the color remain even after the densification of the glass part, resulting in a red-stained glass. Using these two inks, we printed a core-shell disk structure with the gold-doped ink forming the core. The ability to print glass with multiple components opens a route toward glasses with designed compositions, such as gradient-index optics.

In conclusion, we have developed a method of 3D-printing silica suspensions that are subsequently densified into transparent silica glass. The inks are tailored to have optimal drying and rheological properties, and when combined with an appropriate heat treatment process, enable the creation of fully dense glass parts such as monoliths, scaffolds, and, to our knowledge, the first ever 3D-printed microfluidic glass part. We have also demonstrated the fabrication of multi-composition glass parts. Recent advances in 3D-printing technologies, such as active mixing,^[30] could be applied to this general process and result in gradient-composition glass structures with tunable optical and mechanical properties. For example, routes toward 3D-patterned glass microfluidic reactors and 3D gradient-index optics become accessible with this new forming and sintering approach.

Experimental Section

Materials: CAB-O-SIL EH-5 amorphous silica nanopowders were obtained from the Cabot Corporation. Tetraglyme was obtained from Sigma-Aldrich. Hydroxyl-terminated PDMS was obtained from Gelest. Silica-coated 20 nm gold nanospheres were obtained from nanoComposix. All materials were used as supplied.

Glass Ink Preparation: 79 wt% Tetraglyme, 1 wt% PDMS, and 20 wt% EH-5 (76 wt% Tetraglyme, 1 wt% PDMS, and 23 wt% EH-5 for gap spanning structures) were initially loaded into a planetary/centrifugal

mixer (Thinky) container. The components were mixed at 2000 RPM for 3 cycles of 30 s each. In between each cycle, the container was tapped to release remaining silica powder from the container side walls. The inks were then loaded into 30 cc Nordson EFD syringe barrels and centrifuged at 4000 RPM for 3 min.

Glass Ink 3D Printing: The ink-loaded syringes were loaded onto a three-axis micropositioning stage (Aerotech). A constant displacement drive was used to deliver the ink through nozzle diameters of either 610 or 250 μm such that the linear feed rate was 10 mm s^{-1} . The structures were printed on a Teflon mesh (McMaster-Carr), which aided in the initial release of the printed structure from the substrate during the drying process.

Glass Densification: The thermal treatment profile is shown in Figure 3. The printed silica green-bodies were placed onto a hot-plate at 100 °C. After 3 h, the printed green bodies were released from the Teflon mesh to reduce any residual stress that could occur due to the adhesion between the green body and the substrate during the drying process. The green bodies were then dried in a box furnace at 100 °C for 110 h. Next, the solvent-free green bodies were heated to 600 °C at a ramp rate of 10 °C min^{-1} and left to dwell for 1 h to burn out remaining organic components. Last, the part was fully densified in a preheated furnace at 1500 °C for 3 min. The parts were then removed and rapidly cooled to room temperature, in air.

Ink Rheology: Rotational rheology measurements were performed on a TA Instruments DHR-1 rheometer, using a 2° cone and plate setup. The temperature of the Peltier plate was kept at 23 °C. Ink viscosities were measured at shear rates ranging from 0.01 to 100 s^{-1} . Oscillatory measurements of the elastic and viscous moduli were performed at a constant frequency of 1 Hz.

Supporting Information

Supporting Information is available from the Wiley Online Library or from the author.

Acknowledgements

This work was performed under the auspices of the US Department of Energy by Lawrence Livermore National Laboratory under Contract 16-SI-003 within the LDRD program LLNL-JRNL-720419.

Conflict of Interest

The authors declare no conflict of interest.

Keywords

3D printing, direct ink writing, glass, silica, sintering

Received: February 28, 2017

Revised: March 22, 2017

Published online: April 28, 2017

- [1] K. S. Elvira, X. C. i Solvas, R. C. R. Wootton, A. J. deMello, *Nat. Chem.* **2013**, 5, 905.
- [2] H.-K. Choi, M. S. Ahsan, D. Yoo, I.-B. Sohn, Y.-C. Noh, J. T. Kim, D. Jung, J. H. Kim, *Proc. SPIE* **2013**, 8923, 89234T.

- [3] L. Gervais, N. de Rooij, E. Delamarche, *Adv. Mater.* **2011**, 23, H151.
- [4] M. Vallet-Regí, E. Ruiz-Hernández, *Adv. Mater.* **2011**, 23, 5177.
- [5] Z. C. Eckel, C. Zhou, J. H. Martin, A. J. Jacobsen, W. B. Carter, T. A. Schaedler, *Science* **2016**, 351, 58.
- [6] X. Zheng, H. Lee, T. H. Weisgraber, M. Shusteff, J. DeOtte, E. B. Duoss, J. D. Kuntz, M. M. Biener, Q. Ge, J. A. Jackson, S. O. Kucheyev, N. X. Fang, C. M. Spadaccini, *Science* **2014**, 344, 1373.
- [7] N. W. Bartlett, M. T. Tolley, J. T. B. Overvelde, J. C. Weaver, B. Mosadegh, K. Bertoldi, G. M. Whitesides, R. J. Wood, *Science* **2015**, 349, 161.
- [8] M. Zarek, M. Layani, I. Cooperstein, E. Sachyani, D. Cohn, S. Magdassi, *Adv. Mater.* **2016**, 28, 4449.
- [9] G. Siqueira, D. Kokkinis, R. Libanori, M. K. Hausmann, A. S. Gladman, A. Neels, P. Tingaut, T. Zimmermann, J. A. Lewis, A. R. Studart, *Adv. Funct. Mater.* **2017**, 1604619.
- [10] L. Huang, R. Jiang, J. Wu, J. Song, H. Bai, B. Li, Q. Zhao, T. Xie, *Adv. Mater.* **2017**, 29, 1605390.
- [11] J. Klein, M. Stern, G. Franchin, M. Kayser, C. Inamura, S. Dave, J. C. Weaver, P. Houk, P. Colombo, M. Yang, N. Oxman, *3D Print. Addit. Manuf.* **2015**, 2, 92.
- [12] Q. Fu, E. Saiz, M. N. Rahaman, A. P. Tomsia, *Mater. Sci. Eng. C* **2011**, 31, 1245.
- [13] G. Marchelli, R. Prabhakar, D. Storti, M. Ganter, *Rapid Prototyping J.* **2011**, 17, 187.
- [14] F. Kotz, K. Plewa, W. Bauer, N. Schneider, N. Keller, T. Nargang, D. Helmer, K. Sachsenheimer, M. Schäfer, M. Worgull, C. Greiner, C. Richter, B. E. Rapp, *Adv. Mater.* **2016**, 28, 4646.
- [15] M. Wozniak, T. Graule, Y. de Hazan, D. Kata, J. Lis, *J. Eur. Ceram. Soc.* **2009**, 29, 2259.
- [16] J. Luo, H. Pan, E. C. Kinzel, *J. Manuf. Sci. Eng.* **2014**, 136, 61024.
- [17] J. Luo, L. J. Gilbert, D. A. Bristow, R. G. Landers, J. T. Goldstein, A. M. Urbas, E. C. Kinzel, *Proc. SPIE* **2016**, 9738, 97380Y; DOI: 10.1117/12.2218137.
- [18] J. E. Smay, G. M. Gratson, R. F. Shepherd, J. Cesarano, J. A. Lewis, *Adv. Mater.* **2002**, 14, 1279.
- [19] J. A. Lewis, *Adv. Funct. Mater.* **2006**, 16, 2193.
- [20] D. J. Lorang, D. Tanaka, C. M. Spadaccini, K. A. Rose, N. J. Cherepy, J. A. Lewis, *Adv. Mater.* **2011**, 23, 5055.
- [21] E. B. Duoss, T. H. Weisgraber, K. Hearon, C. Zhu, W. Small, T. R. Metz, J. J. Vericella, H. D. Barth, J. D. Kuntz, R. S. Maxwell, C. M. Spadaccini, T. S. Wilson, *Adv. Funct. Mater.* **2014**, 24, 4905.
- [22] C. Zhu, T. Y.-J. Han, E. B. Duoss, A. M. Golobic, J. D. Kuntz, C. M. Spadaccini, M. A. Worsley, *Nat. Commun.* **2015**, 6, 6962.
- [23] A. R. Hamilton, N. R. Sottos, S. R. White, *Adv. Mater.* **2010**, 22, 5159.
- [24] Q. Fu, E. Saiz, A. P. Tomsia, *Adv. Funct. Mater.* **2011**, 21, 1058.
- [25] T. Suratwala, Z. Gardlund, K. Davidson, D. R. Uhlmann, S. Bonilla, N. Peyghambarian, *J. Sol-Gel Sci. Technol.* **1997**, 8, 953.
- [26] K. Kajihara, *J. Asian Ceram. Soc.* **2013**, 1, 121.
- [27] C. Zhu, J. E. Smay, *J. Rheol.* **2011**, 55, 655.
- [28] Q. Liu, A. A. Patel, L. Liu, *ACS Appl. Mater. Interfaces* **2014**, 6, 8996.
- [29] S. Link, M. A. El-Sayed, *J. Phys. Chem. B* **1999**, 103, 8410.
- [30] T. J. Ober, D. Foresti, J. A. Lewis, *Proc. Natl. Acad. Sci. USA* **2015**, 112, 12293.